The Active Center of a Mammalian α-Amylase. Structure of the Complex of a Pancreatic α-Amylase with a Carbohydrate Inhibitor Refined to 2.2-Å Resolution[†,‡]

Minxie Qian,[§] Richard Haser,[§] Georges Buisson,[⊥] Emile Duée,[⊥] and Françoise Payan*[,§]

LCCMB-CNRS, URA 1296, Faculté de Médecine Nord Bd Pierre Dramard, 13916 Marseille Cedex 20, France, and LCM, IBS, 38027 Grenoble Cedex 1, France

Received December 2, 1993; Revised Manuscript Received March 7, 1994[⊛]

ABSTRACT: An X-ray structure analysis of a crystal of pig pancreatic α-amylase (EC 3.2.1.1) that was soaked with acarbose (a pseudotetrasaccharide α-amylase inhibitor) showed electron density corresponding to five fully occupied subsites in the active site. The crystal structure was refined to an *R*-factor of 15.3%, with a root mean square deviation in bond distances of 0.015 Å. The model includes all 496 residues of the enzyme, one calcium ion, one chloride ion, 393 water molecules, and five bound sugar rings. The pseudodisaccharide acarviosine that is the essential structural unit responsible for the activity of all inhibitors of the acarbose type was located at the catalytic center. The carboxylic oxygens of the catalytically competent residues Glu233 and Asp300 form hydrogen bonds with the "glycosidic" NH group of the acarviosine group. The third residue of the catalytic triad Asp197 is located on the opposite side of the inhibitor binding cleft with one of its carbonyl oxygens at a 3.3-Å distance from the anomeric carbon C-1 of the inhibitor center. Binding of inhibitor induces structural changes at the active site of the enzyme. A loop region between residues 304 and 309 moves in toward the bound saccharide, the resulting maximal mainchain movement being 5 Å for His305. The side chain of residue Asp300 rotates upon inhibitor binding and makes strong van der Waals contacts with the imidazole ring of His299. Four histidine residues (His101, His201, His299, and His305) are found to be hydrogen-bonded with the inhibitor. Many protein–inhibitor hydrogen bond interactions are observed in the complex structure, as is clear hydrophobic stacking of aromatic residues with the inhibitor surface. The chloride activator ion and structural calcium ion are hydrogen-bonded *via* their ligands and water molecules to the catalytic residues.

α-Amylase (α-1,4-glucan-4-glucanohydrolase, EC 3.2.1.1) catalyzes hydrolysis of α-(1,4) glycosidic linkages of starch components, glycogen, and various oligosaccharides. In mammals, α-amylase is present in both salivary and pancreatic secretions. Amino acid sequence comparison of porcine, human, mouse, and rat pancreatic amylase shows a high degree of homology (Pasero *et al.*, 1986), e.g., between human and hog the homology is 84% (Qian *et al.*, 1993). Two refined three-dimensional structures have been reported for fungal α-amylases: *Aspergillus niger* acid amylase (Brady *et al.*, 1991) and *Aspergillus oryzae* (TAKA) amylase (Swift *et al.*, 1991). One refined three-dimensional structure has been recently reported for a mammalian α-amylase from pig pancreas (Qian *et al.*, 1993).

Porcine pancreatic α-amylase (PPA)[1] is an endo-type amylase. It catalyzes the hydrolysis of internal α-(1,4) glucosidic bonds in amylose and amylopectin through multiple attack toward the nonreducing end (Robyt & French, 1970a; Prodanov *et al.*, 1984). Two isoenzymes (PPA I and II) are known for pig pancreatic α-amylase (Marchis-Mouren & Pasero, 1967). They have the same molecular weight but differ slightly in amino acid composition and isoelectric point (Pasero *et al.*, 1986; Kluh, 1981).

The enzyme requires one essential calcium ion (Steer & Levitzki, 1973; Vallee *et al.*, 1959) for its structural integrity, and it is activated by chloride ions (Levitski & Steer, 1974); maximal enzymatic activity occurs around pH 7 (Thoma, 1968; Wakim *et al.*, 1969; Thoma *et al.*, 1971; Ishikawa *et al.*, 1993). Based upon kinetic studies of the action pattern (Robyt & French, 1970a), it is suggested that the active site of the pig pancreatic α-amylase contains five subsites for binding of glucose units, the catalytic attack occurring between subsites 3 and 4, which is shown in Figure 1a. The maltopentaose and higher maltodextrin molecules are good hydrolytic substrates (Robyt & French, 1970a). The catalytic efficiency (k_{cat}/K_m) increases with chain length from 2 M^{-1} s^{-1} for maltose up to 1.10^7 M^{-1} s^{-1} for 410-residue amylose (Marchis-Mouren & Desseaux, 1989). Maltotriose and maltotetraose molecules are considered poor substrates which usually undergo the so-called "bireactions" such as condensation during the hydrolysis process. Low-resolution X-ray studies using PPA isozyme I crystals soaked with methyl and nitrophenyl thiomaltoside revealed two binding sites per molecule for short substrate analogues and localized the active site (Payan *et al.*, 1980).

The three-dimensional molecular model of PPA has recently been described in detail; the chloride and calcium binding sites have been characterized (Qian *et al.*, 1993). This refined model shows the three residues Asp197, Glu233, and Asp300 close together in the active site. According to sequence

[†] This work has been supported by the CNRS-IMABIO program, by BAYER AG, and by the PACA region.

[‡] Crystallographic coordinates for the acarbose/PPA complex have been submitted to the Brookhaven Protein Data Bank under filename 1PPI.

* Author to whom all correspondence should be addressed.

[§] LCCMB-CNRS.

[⊥] LCM.

[⊛] Abstract published in *Advance ACS Abstracts,* April 15, 1994.

[1] Abbreviations used: PPA, pig pancreatic α-amylase; HPA, human pancreatic α-amylase; TAKA-amylase, *Aspergillus oryzae* α-amylase; CGTase, cyclodextrin glucanotransferase; G, glucose unit; rms, root mean square; σ, standard deviation.

0006-2960/94/0433-6284$04.50/0

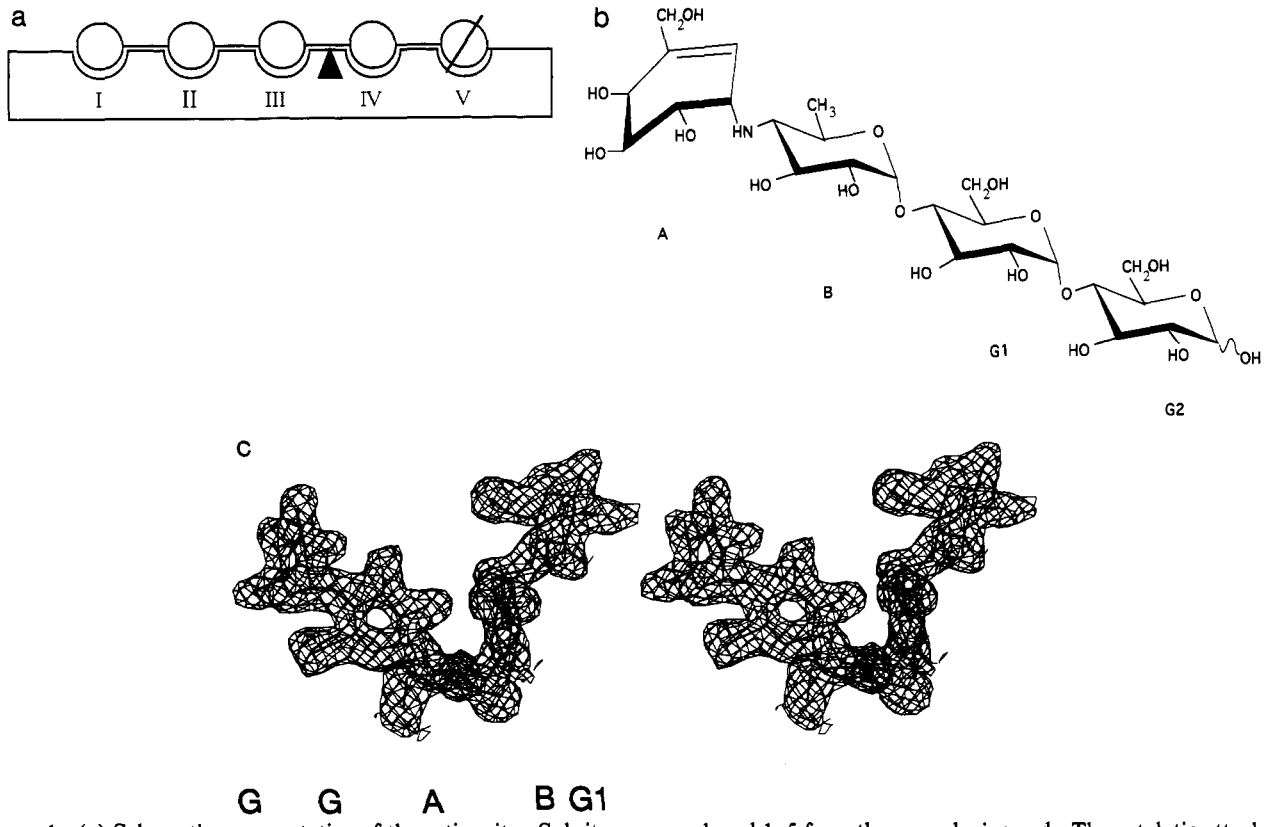

FIGURE 1: (a) Schematic representation of the active site. Subsites are numbered 1–5 from the nonreducing end. The catalytic attack (▲) occurs between subsites 3 and 4. The glucose reducing end (∅) is represented in subsite 5. Subsite 3 is known as the catalytic subsite (Chan *et al.*, 1984; Braun *et al.*, 1985a,b; Marchis-Mouren & Desseaux, 1989). (b) Structure of acarbose (Schmidt *et al.*, 1977). The cyclitol unit is labeled A, the amino sugar unit is labeled B, and the two glucose units are labeled G1 and G2. The trivial name for the entity consisting of units A–B is acarviosine. (c) Stereoscopic view of the final $(2F_{obs} - F_{calc})$ $\exp(i\alpha_{calc})$ electron density map of the bound acarbose inhibitor at 2.2-Å resolution. The labeling of the different units occupying the electron density is G for glucose and AB for acarviosine.

comparisons (MacGregor & Svensson, 1989) and X-ray studies, homologous residues have been identified in the TAKA-amylase active site (Asp206, Glu230, Asp297; Matsuura *et al.*, 1984), in barley α-amylase (Asp179, Glu204, Asp289; Kadziola, 1993), and in *Bacillus circulans* CGTase, (Asp229, Glu257, Asp328; Klein *et al.*, 1992). The refined PPA structure shows a network of water molecules occupying the cleft of the active site and hydrogen-bonding with polar side chains of Asp300, Glu233, and Asp197, with the chloride ligand Asn298, and with the main chain through Ala307 N and Trp59 O. Also present in the cleft are aromatic residues such as Trp58, Trp59, and Tyr62. The loop region between residues 304 and 309 surrounds the active site from one side and displays high *B*-factors.

In the present study, the three-dimensional structure of native PPA soaked with a carbohydrate α-amylase inhibitor (acarbose) has been determined to 2.2-Å resolution. Our X-ray analysis revealed a well-defined density corresponding to five fully occupied subsites in the active site. The X-ray model clearly presents a subset of residues directly involved in binding the inhibitor and/or in position to assist catalysis and locates the activator chloride ion in close proximity to the inhibitor.

MATERIALS AND METHODS

Crystals of native PPA isozyme I used in this study were identical to those previously reported for the native structure determination (Qian *et al.*, 1993). The carbohydrate inhibitor acarbose was kindly provided by Dr. H. Bischoff (Bayer AG). The acarbose molecule has a pseudotetrasaccharide structure, as shown in Figure 1b. A branched unsaturated cyclitol is connected *via* an amino group to 4-amino-4,6-dideoxy-D-glucose, which itself is linked by an α-(1,4)-*O*-glycosidic bond to a maltose unit. The K_i constant value of the bound acarbose to PPA is 9.7×10^{-6} M (Wilcox & Whitaker, 1984).

The active center of PPA is not blocked in the crystal packing and can be easily accessed by external ligands (Payan *et al.*, 1980). This allows one to obtain enzyme–inhibitor complexes by soaking native crystals in buffered crystal-stabilizing solutions of the compound of interest. The previous soaking conditions used with modified maltotriose (Payan *et al.*, 1980) could not be applied with acarbose because of severe crystal deterioration. In the present study, complexes were formed by soaking crystals for 48 h at 20 °C in a solution containing 1 mM acarbose in Tris buffer 0.01 M, 1 mM $CaCl_2$, 2 M NaCl at pH 8.

As for the native crystals (Qian *et al.*, 1993), data collection was carried out at the NIH national research resource (UCSD) on a Hamlin/Xuong area detector (Hamlin, 1985) mounted on a Rigaku rotating anode X-ray generator (Cu Kα radiation, 50 kV, 100 mA, graphite monochromator). Table 1 summarizes statistics for the data sets on the free and acarbose-complexed PPA.

Crystals of the inhibitor complex were isomorphous to those of the native enzyme and diffracted equally well. The data were 95% complete to 2.06-Å resolution, the average overall and final shell I/σ values being equal to 21.3 and 9.9, respectively. The refinement was based on 25 018 independent reflections in the 8–2.2-Å resolution range. The data collected for the inhibitor complex were scaled against those for the native PPA crystals and analyzed using the program packages PROTEIN (Steigemann, 1974) and CCP4 (CCP4 Program Suite, Daresbury Laboratories).

Table 1: Statistics of Data Collection and Refinement

	native	complex
cell parameters ($P2_12_12_1$)		
a (Å)	56.3	56.2
b (Å)	87.8	87.7
c (Å)	103.4	103.6
resolution limit (Å)	2.06	2.06
no. measurements	111 419	93 924
no. unique reflctns	30 390	29 214
completeness of data set (%)	99	95
R_{sym}[a]	4.07	3.6
refinement range (Å)	8–2.1	8–2.2
no. reflctns in refinement	29 838	25 018
R-factor (%)[b]	15.6	15.4
no. protein atoms	3910	3910
no. inhibitor atoms		55
no. water molecules	353	393
rms deviations		
bond lengths (Å)	0.014	0.015
angles (deg)	2.8	2.9

[a] R_{sym} is defined as $\sum_{i,hkl}|I(i,hkl) - \langle I(hkl)\rangle|/\sum_{i,hkl}I(i,hkl)$, where i runs through the symmetry-related reflections. [b] The crystallographic R is defined as $\sum||F_o| - |F_o||/\sum|F_o|$.

The $(F_{obs,complex} - F_{obs,native})\exp(i\alpha_{calc,native})$ map calculated between 25- and 2.2-Å resolution showed continuous, well-defined, strong electron density in the active site cleft, corresponding to five fully occupied subsites. Initial phases for the complex ($\alpha_{calc,native}$) were calculated from the completely refined model of the native enzyme (Qian *et al.*, 1993).

For refinement we used the simulated annealing program XPLOR (Brünger *et al.*, 1987) and followed a protocol similar to the one for native PPA (Qian *et al.*, 1993). The procedure started with the refined structure of uncomplexed PPA, with 13 water molecules deleted which overlapped with the observed initial difference Fourier density in the active site region. The template of a glucose residue for refinement of the inhibitor structure was taken from crystallographic data for individual monosugars, and that for the acarviosine entity (cyclitol and amino sugar units) was taken from Bock and Pedersen (1984). All model construction and structure comparison work used the program TURBO implemented on a Silicon Graphics 4D/380 computer (Roussel & Cambillau, 1989).

The shape of the initial density enabled us to determine unambiguously the location in subsite 4 of the amino sugar residue (residue B in Figure 1b), in which the C-6 hydroxyl group was missing, and to assign the chain direction based upon the densities corresponding to hydroxyl O-6 oxygen atoms of the other residues. Subsequently, residues A and G1 of the initial acarbose structure could be identified, bound at subsites 3 and 5. At the position corresponding to the fourth acarbose residue, no density was observed, while two additional glucose rings apparently were present at the opposite end of the chain in subsites numbered 1 and 2 according to the notations of Figure 1a.

At first only the three identified units of acarbose (named A, B, and G1 in Figure 1b) were introduced in the refinement procedure. After the first cycle, a strong, continuous electron density was observed beyond the cyclitol ring which was consistent with a maltosyl unit connected to the cyclitol ring by an α-(1,4)-*O*-glycosidic bond; the possibility of fitting two separate molecules to the observed density was checked and rejected. The five-unit inhibitor molecule was used and confirmed by the subsequent refinement.

All solvent molecules with densities below 1σ in the $(2F_{obs} - F_{calc})\exp(i\alpha_{calc})$ map and temperature factors above 70 Å^2 were removed after the first iteration of refinement. The difference electron density maps also revealed 40 additional water molecules. The new sites were added to the model, provided that the electron density was present at a level of at least 3.5σ in the $(F_{obs} - F_{calc})\exp(i\alpha_{calc})$ maps. The molecules introduced were inspected visually for correct geometry of hydrogen-bonding and were given an initial B-factor of 20 A^2.

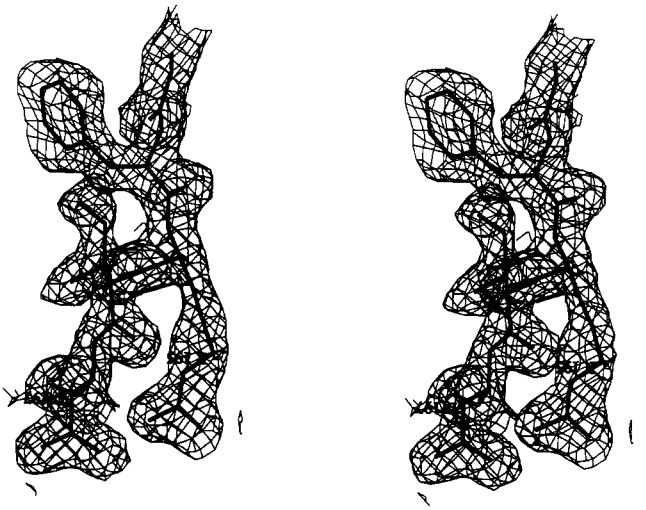

FIGURE 2: Quality of the final $(2F_{obs} - F_{calc})\exp(i\alpha_{calc})$ electron density map at 2.2-Å resolution as exemplified at residues 194–197 of the active site.

When the R-factor[2] reached 15.3% in the range 8.0–2.2 Å for 25018 reflections, with a model obeying standard geometry within 0.015 Å in bond lengths and 2.9° in bond angles, and the $(F_{obs} - F_{calc})\exp(i\alpha_{calc})$ map showed no more interpretable features, refinement was halted, yielding a model consisting of 3914 protein atoms (i.e., all non-hydrogen atoms), one Ca ion, one Cl ion, 55 inhibitor atoms, and 393 water molecules.

RESULTS

(a) Difference Electron Density Map and Quality of the Model. In order to substantiate the further discussions on enzymatic mechanism and details of the interactions between enzyme and inhibitor, it is important to verify the quality of the structures on which this discussion is to be based. Initial difference Fourier showed clear density in the active site cavity corresponding to the ligand, while no electron density was found in the second binding site, which was identified in our low-resolution studies of PPA (Payan *et al.*, 1980) with maltotriose analogues. The density in the active center was strong, and the five subsites were fully occupied. As explained above, the shape of the density enabled us to identify the 6-desoxypranose unit and to determine the chain direction. The final electron density map and the structure of the inhibitor are shown in Figure 1c.

At the 1σ level of the final $(2F_{obs} - F_{calc})\exp(i\alpha_{calc})$ map, all protein and inhibitor atoms have well-defined density except, as in the native structure, for the first two residues at the N-terminus. The quality of the model is demonstrated in Figure 2, showing the observed electron densities for the side chains of residues in the active site region.

All protein residues that directly contact the bound pseudopentasaccharide are very clearly observed in the electron density maps, as are the water molecules. It is noteworthy that His305, located in the active site cleft, exhibits a well-defined strong density and a lower temperature factor in the inhibitor complex structure. The increased order for this residue is indicative of its participation in the inhibitor binding.

Most residues found to be disordered in the native structure (Qian *et al.*, 1993) remain disordered in the inhibitor complex.

[2] R-factor = $\sum||F_{obs}| - |F_{cal}||/\sum|F_{obs}|$.

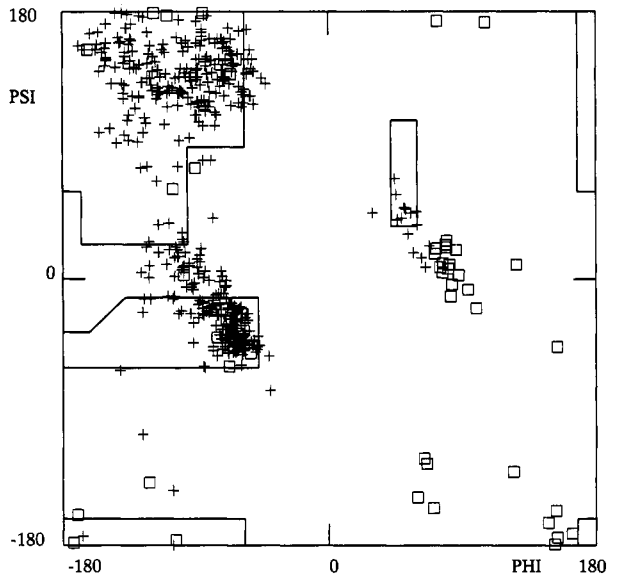

FIGURE 3: Distribution of main-chain dihedral angles for acarbose complex. +, Non-glycine residues; □, glycine residues. The preferred regions as outlined by Ramanchandran and Sasisekharan (1968) are indicated.

However, better defined electron density for the residues Asn53, Met82, Glu369, and Gln435 is observed in the liganded form of the enzyme. This result may be related to an increased overall stability of the complex, as illustrated by the lower average *B* value of 12.5 Å^2 for the complexed structure, compared to the average *B*-factor value of 14.1 Å^2 for the free enzyme structure.

Thermal parameters for the bound sugar ring atoms differ slightly between subsites and are of a magnitude similar to those of the protein atoms involved in the interaction. In subsites 1 and 5 of the active site sugar unit, atoms exhibit the highest *B* values, ranging from 9 to 18 Å^2. Thermal parameters for atoms of the acarviosine entity that occupies subsites 3 and 4 range from 2 to 6 Å^2 for the cyclitol ring (subsite 3) and from 6 to 13 Å^2 for the amino sugar (subsite 4). The clear density and the low *B*-factor values indicate high order and strength of the inhibitor binding interactions.

A good indicator for the stereochemical correctness for the model is provided by a (ϕ,ψ) scatter plot (Ramachandran & Sasisekharan, 1968) Figure 3 displays the (ϕ,ψ) angles for the refined inhibitor complex. Most of the residues fall in energetically preferred regions with a few exceptions, which are the same as in the native enzyme structure (Qian *et al.*, 1993). The torsion angles at the α-(1,4)-*O*-glycosidic bonds connecting sugar residues are close to the minimum energy values allowing formation of O2–O3 hydrogen bonds between adjacent sugar residues, which is characteristic of maltose and amylose crystals.

(b) Conformational Changes in the Enzyme. The overall conformation of PPA in the complex is essentially the same as in the native structure (Qian *et al.*, 1993), with an average rms deviation value of 0.28 Å. Large deviations are observed only in the region between residues 304 and 309 (Figure 4). This segment corresponds to the flexible loop identified in the native structure (Qian *et al.*, 1993). The moving loop has a glycine-rich sequence Gly-His-Gly-Ala-Gly-Gly-Ser, which clearly indicates its flexibility and strongly suggests that its motion may be important for enzyme function. In the native structure this fragment of sequence was distinguished as one of the regions characterized by the highest temperature factors (Qian *et al.*, 1993). With the bound inhibitor, *B*-factors of Gly304 and His305 are reduced from 25 and 35 Å^2 to 5 and 8 Å^2, respectively. In the rest of the loop, the *B*-factors, ranging from 15 to 32 A^2, remain similar to those observed in the native enzyme for the corresponding residues.

Displacement of the loop in response to the inhibitor binding can be seen in Figure 5. It moves toward the saccharide, thus reducing the cleft breadth. The maximum main-chain movement is 5 Å at His305, which approaches the inhibitor from the solvent side and makes a good hydrogen bond with the residue in subsite 2. As a result, the loop 304–309 in the complex forms the surface edge of the cleft, being involved in the architecture of subsites 2, 4, and 5. Subsite 3 is deeper in the cleft, while the residue in subsite 1 is above the loop and

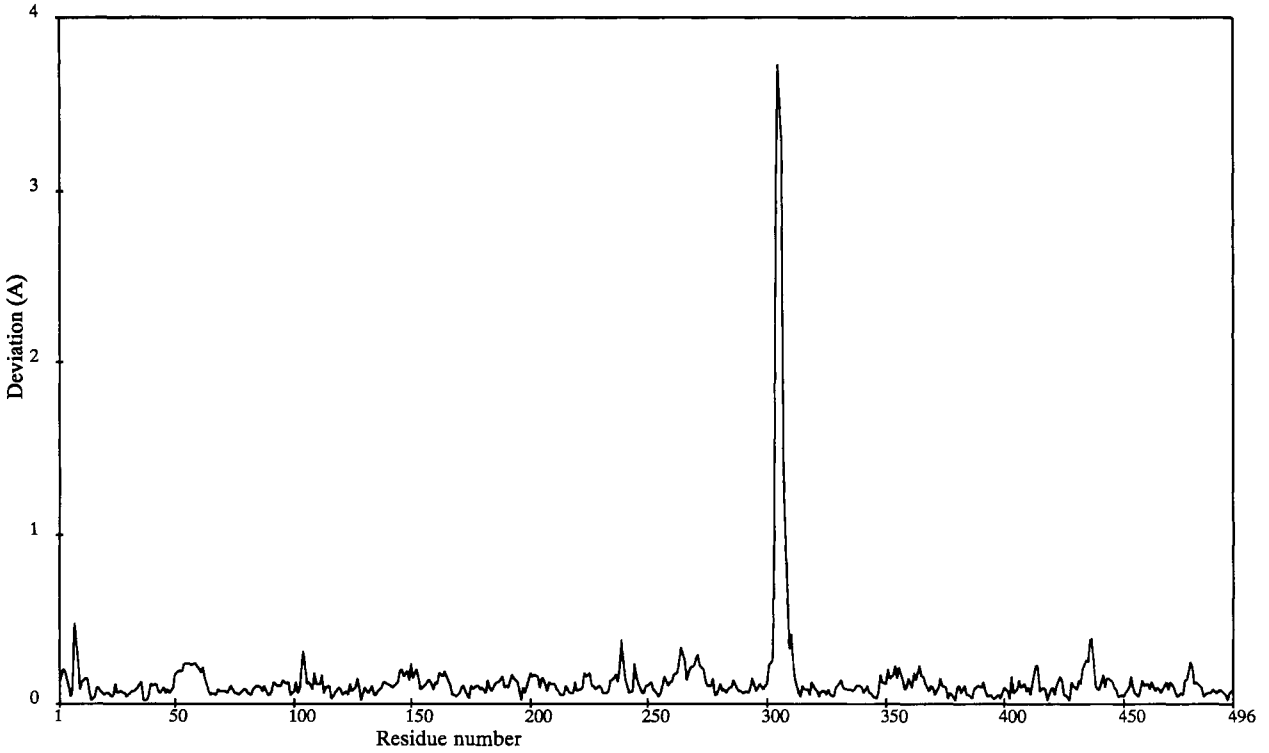

FIGURE 4: Root mean square deviation between corresponding main-chain atoms of the free and complexed structures of PPA.

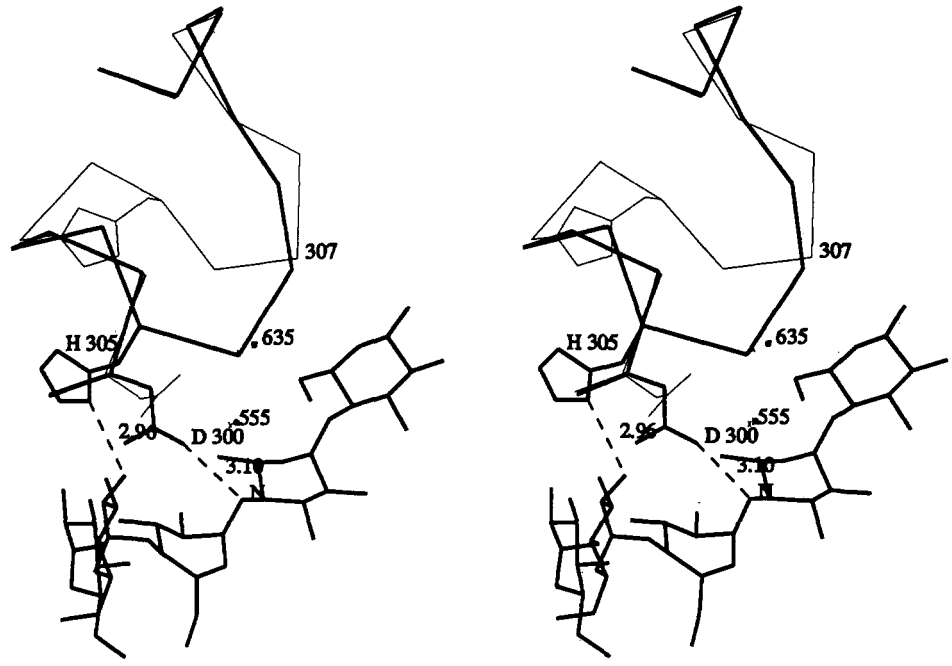

FIGURE 5: Stereoscopic view of the superimposition of the α-carbon backbone traces in the region of the flexible loop (between residues 300 and 312) for free and acarbose-complexed PPA. The thick lines correspond to the structure of the complex. For clarity, only the side chains of His305 and Asp300 which move significantly upon inhibitor binding are shown.

Table 2: Hydrogen Bonds in the Active Site of PPA/Acarbose Complex

	direct hydrogen bond to protein			water-mediated hydrogen bond to protein					
subsite[a]	substrate atom	protein atom	*d* (Å)	substrate atom	water atom	*d* (Å)	water atom	protein atom	*d* (Å)
1	O-4	Val163 O	2.72	O-2	O-892[b]	2.62			
	O-5	Gln63 NE2	3.18	(O-892*)	O-752	2.72	O-752	Asp356 OD1	2.82
	O-6	Asp165 OD2	3.03				O-752	Trp59 NE1	3.12
	O-6	Val163 O	2.91						
2	O-2	His305 ND1	2.97	O-3	O-659	2.84			
	O-6	Gln63 NE2	2.88	(O-659)	O-764	2.89	O-764	Gly306 N	2.93
	O-6	Trp59 O	2.76	(O-764)	O-943*	2.91	O-943	Gly304 O	2.96
3	O-2	Asp300 OD1	2.85						
	O-2	His299 NE2	3.13						
	O-3	His299 NE2	2.98						
	O-3	Asp300 OD2	2.91						
	O-6	Asp197 OD1	2.71						
	O-6	His101 NE2	2.73						
4	O-2	His201 NE2	2.66	O-2	O-610	3.20	O-610	Glu233 O	3.28
	O-3	Glu233 OE2	2.76	O-3	O-610	3.14			
	N-4	Glu233 OE1	2.94	O-5	O-930*	2.99			
	N-4	Asp300 OD1	3.07						
5	O-2	Glu240 OE1	2.78	O-1	O-883*	3.12	O-883	Gly306 O	3.25
	O-2	Lys200 NZ	2.74	O-5	O-883	3.21			
	O-3	Lys200 NZ	3.21	O-2	O-897*	2.84			
				(O-897)	O-690	2.75	O-690	Gly238 O	2.92
				O-6	O-930*	3.08			
				(O-930)	O-659	2.96			
				(O-659)	O-764	2.89			

[a] Numbered 1–5 from the nonreducing end. [b] O-*xxx*, water molecule; *, only present in the complexed state.

more exposed to the solvent. The described conformational changes are accompanied by minor readjustment of the surrounding side chains.

The second important difference between the free and liganded enzyme structures is found for Asp300, which is also shown in Figure 5. Though not part of the flexible loop, the side chain of this residue adopts a distinctly different position in the complex by rotating approximately 60° around the CA–CB bond. As a result, the carboxyl group gets somewhat deeper into the cleft, and its OD2 oxygen earlier exposed to the solvent makes a strong hydrogen bond with the cyclitol residue in subsite 3. In the free enzyme, OD1 of this carboxyl is involved in a hydrogen-bond network with solvent molecules bound in the cleft (Qian *et al.*, 1993). Namely, two water molecules (635 and 555, Figure 6a) bridge across the cleft from carboxyl of Glu233 to amide of Asn298 and to the main-chain NH group of Ala307. In the complex (Figure 6b) this bridging remains intact, but OD1 of Asp300 switches its hydrogen-bonding from water 635 to 555. At the same time, water 635 keeps its hydrogen bond with the main-chain NH group of Ala307 of the flexible loop. Upon inhibitor binding, the orientation of the Asp300 side chain becomes similar to that observed for the homologous residue in the free TAKA-amylase structure (Swift *et al.*, 1991).

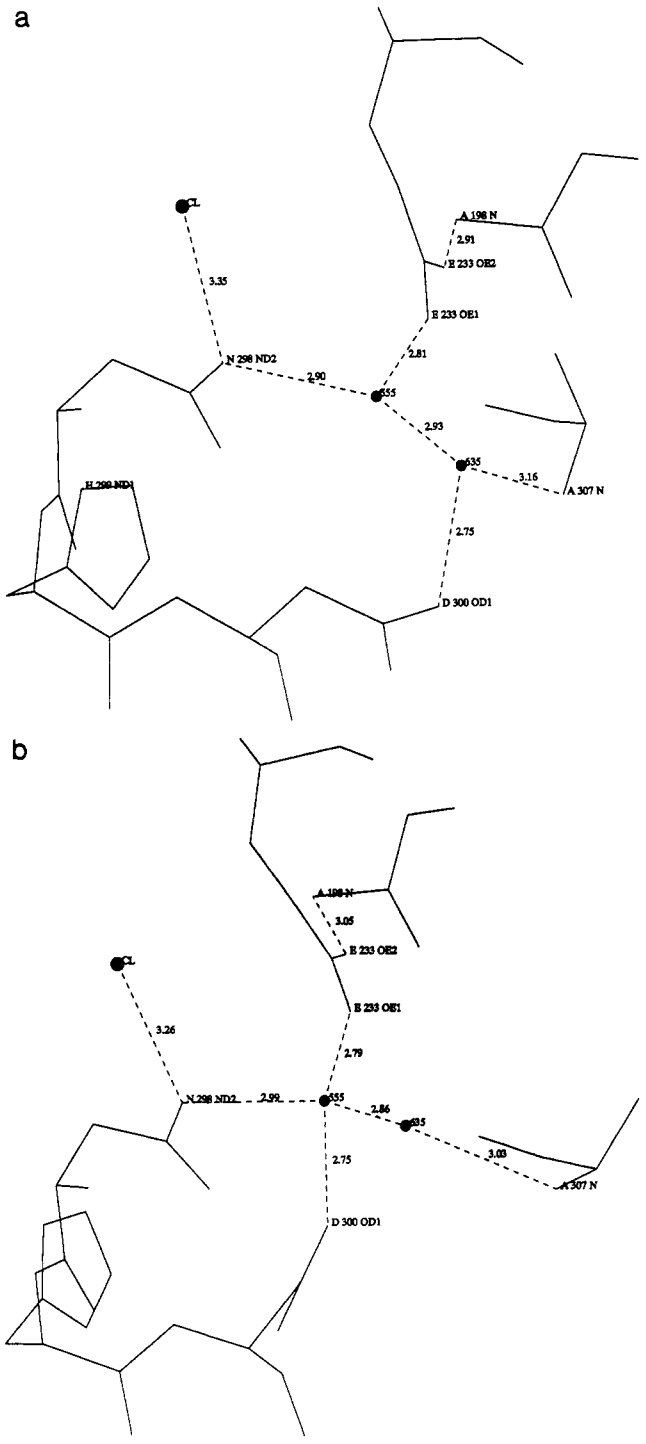

FIGURE 6: Hydrogen-bonding involving water molecules in the immediate environment of the catalytic residues Asp300 and Glu233 for the free PPA structure (a) and for the complexed structure (b). ●, Water molecules. Dashed lines represent hydrogen bond lengths and also the interaction between the chloride ion and one of its ligands, Asn298 ND2.

Inspection of the solvent molecules observed in the active site cleft in the free and complexed states indicates that the inhibitor substitutes 10 ordered water molecules at subsites 2, 3, and 4. No ordered water was found in subsites 1 and 5 in the free enzyme (Qian *et al.*, 1993). Several water molecules are buried inside the protein in the vicinity of the binding cleft, near the calcium and chloride binding sites. Four of them (525, 555, 610, and 635), already present in the free enzyme structure, are close to the inhibitor molecule. Table 2 and Figure 8 show that among the ordered water molecules mediating hydrogen bonds between carbohydrate and protein, five of them are new molecules accompanying the sugar residues. Upon inhibitor binding, water 635, which in the free structure is directly hydrogen-bonded to Asp300, is shifted at about 1 Å, while waters 555 and 525 keep their positions and orientations. The geometries of both the Cl^- and the Ca^{2+} binding sites remain intact upon inhibitor binding. In terms of *B*-factors within the active site, some significantly lower values are observed. The ordering of the flexible loop is described above. The thermal parameter values for the side chain of the residue Asp300 are very different in the native and complex structures, 27 and 8 Å^2, respectively. The *B*-factor of water 555 is reduced from 13.9 to 3.8 Å^2. Better ordering is also observed for histidine 305 with an enhanced electron density. His299, His201, and His101, also located in the active center, show lower *B*-factor values than in the native enzyme three-dimensional structure.

(c) Enzyme–Inhibitor Interactions in the Active Center. The current study reveals in detail the interactions between the carbohydrate inhibitor and the mammalian α-amylase. Figure 7 shows arrangement of protein side chains involved in interaction with the inhibitor. Table 2 lists major contacts in each of the five subsites where inhibitor residues are bound. A schematic diagram is shown in Figure 8.

The active site region is a V-shaped depression located at the carboxyl end of the domain A β-barrel. The walls of this V-shaped cavity are mainly composed of the loops between the third β-strand and the third α-helix and between the seventh β-strand and the seventh α-helix of the barrel. The catalytic region surrounding the catalytic subsite number 3 (Chan *et al.*, 1984; Braun *et al.*, 1985a,b; Marchis-Mouren & Desseaux, 1989) is situated in the heart of the cavity. In the complex structure, the third subsite is occupied by the cyclohexene ring. The half-chair conformation of this moiety is thought to act as a transition-state analogue of the putative oxocarbonium ion intermediate of glycosidase catalysis (Schmidt *et al.*, 1977; Goldsmith *et al.*, 1987). It appears to be surrounded by the three carboxyl groups of Glu233, Asp300, and Asp197. All of them show well-defined orientations with respect to the nitrogen atom that corresponds to the glycosidic oxygen in substrate structures. This arrangement unequivocally points to the place of the catalytic attack.

Oxygens OE1 of Glu233 and OD1 of Asp300 flank the nitrogen that connects rings 3 and 4 of the inhibitor molecule, making two hydrogen bonds of lengths 2.9 and 3.1 Å, respectively. Asp197 is close to these two, but it lies opposite in the cleft at a distance of 3.3 Å from the anomeric carbon C-1 of the cyclitol unit. This structural arrangement suggests important roles of the three residues in the catalytic process. However, several other residues in the active center of PPA probably are also of importance. In the third subsite, Tyr62, which is more deeply located in the reaction center, stacks onto the cyclitol ring. The overall bending of the bound inhibitor chain looks like a kink in the sugar chain and is caused by a flip of ring surfaces between subsites 3 and 4.

Of the four histidines present in the active center pocket, His101 and His299 are involved in the interactions in the catalytic subsite. His101 is hydrogen-bound to the C-6 hydroxyl group of cyclitol, while His299 makes hydrogen bonds with O-2 and O-3 of the same residue (Figure 8). His299 in the liganded structure is very close to Asp300, making several van der Waals contacts. However, no good direct hydrogen-bonding of the two histidines with catalytic carboxyl groups is observed. The two possible orientations of the histidine ring about the CB–CG bond are indistinguishable in the electron density map; the choice of the rotation state is clear for His299, but for His101, hydrogen bonds are possible for both alternative orientations of the imidazole ring. The

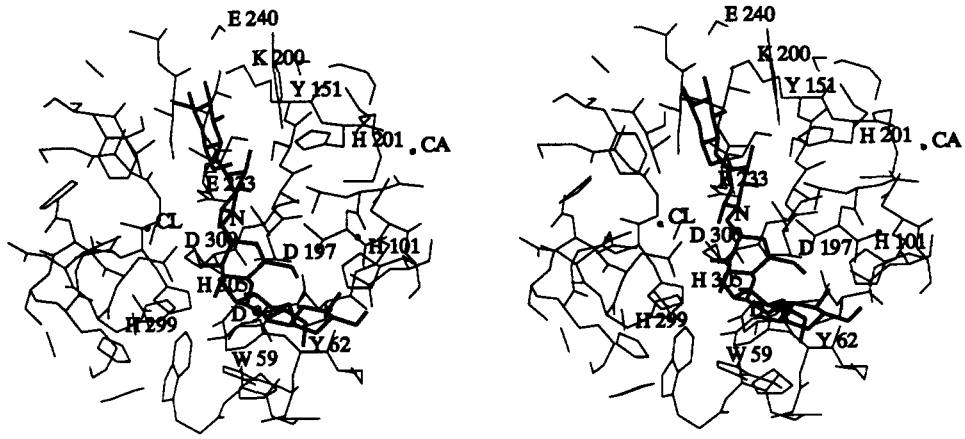

FIGURE 7: Detailed stereoview of the PPA active site with the acarbose ligand bound.

selected orientation for His101 is based on the better geometry of the two hydrogen bonds formed by the nitrogen atoms of the imidazole ring. In the most probable conformation (Figure 8), the His101 ND1 atom is at a hydrogen-bonding distance (3.1 Å) with the side-chain nitrogen of the calcium ligand Asn100. Thus, His101 appears to be in a close though indirect contact with the Ca ion. His299 is in a similar contact with the Cl ion *via* a strong hydrogen-bonding with water 525 (Figure 8). In both cases histidines appear to be hydrogen-bonded with inhibitor hydroxyl groups, which at the same time make hydrogen bonds with carboxyl oxygens of the catalytic residues. Indeed the above histidine residues have been shown to play important roles in the catalytic function of PPA and other amylolytic enzymes (Ishikawa *et al.*, 1993; Nakamura *et al.*, 1993). His201 is involved in inhibitor binding in subsite 4, where it makes a good hydrogen bond with O-2 of the amino sugar. The fourth histidine in the active center, His305, is involved in the loop motion described above, and it makes a hydrogen bond with the sugar residue in subsite 2.

Although many protein–inhibitor hydrogen bonds are observed in the complex structure, it should be noted that, as usually observed in protein–carbohydrate interactions (Vyas, 1991), a substantial part of the hydrogen-bonding potential of sugar residues is engaged in interactions with solvent water. Another major feature of the protein–sugar interactions already analyzed (Quiocho, 1989) is observed in the present complex: significant nonpolar enzyme–inhibitor interactions are found in each subsite of the active center. In subsites 1, 2, and 5 there is clear hydrophobic stacking of aromatic residues Trp58, Trp59, Tyr62, and Tyr151, with inhibitor surface below α-(1,4)-*O*-glycosidic bonds, which are known to exhibit hydrophobic properties (Johnson *et al.*, 1988). The phenol rings of Tyr151 and Tyr62 and the indole ring of Trp59 are nearly parallel to the inhibitor's surface (see Figure 9 for Trp59). In subsite 4, a similar interaction with side chains of Leu162 and Val163 is observed.

(d) Chloride and Calcium Binding Sites. As noted above, no significant changes in the positons and orientations of protein groups and bound water molecules around Ca and Cl ions are observed. The chloride ion lies at a distance of 7.0 Å from the point of the catalytic attack represented by the NH glycosidic bond. Its ligands (Arg195, Asn298, Arg337, and water 525) form an extensive hydrogen bond network in which the catalytic residues are also involved (Figure 8b). Arg195 is hydrogen-bonded with OD2 of Asp197. Asn298 interacts with carboxyl groups of both Glu233 and Asp300 *via* a chain of two strong hydrogen bonds mediated by water 555. Water 525 is hydrogen-bonded to the imidazole ring of histidine 299, which strongly interacts with the side chain of Asp300. This conspicuous arrangement of residues associated with the Tyr62 forms an anchorage "platform" for the catalytic subsite in the heart of the V-shaped cavity where the substrate used to fit, and the chloride ion is nestled in the vicinity.

The calcium ion is 12.4 Å apart from the point of the catalytic attack. Figure 8b shows the pathway of the most intimate contacts between Ca ion, catalytic center, and Cl ion. The main-chain NH group of the Ca ion ligand Asn100 is hydrogen-bonded *via* a water molecule with OD1 of the catalytic Asp197, which in turn interacts with Cl^- *via* OD2 as described above. Thus, residue Asp197 appears to be positioned in the proximity of both the chloride and the calcium ions. Subsites 4 and 5 of the active center are closer to the Ca ion than the rest of the binding regions. His201 is liganded with Ca ion *via* its main-chain carbonyl oxygen and is also strongly hydrogen-bonded to the fourth inhibitor residue (Figure 8).

DISCUSSION

(a) Acarbose in the Active Site of PPA. The results reported here suggest that PPA in the crystal is able to transform the initial acarbose molecule structure (Figure 1b), thus giving a five-unit product as present in Figure 1c. In fact, this effect was very advantageous for the present work because it allowed us to scrutinize interactions in all five subsites of the active center. This result, however, is very striking, because normally hydrolases destroy substrate analogues or inhibitors added, and we are not aware of any similar examples in the literature.

It was shown that pancreatic amylases can cleave the reducing end glucose unit from acarbose, while no other bonds are hydrolysable (Müller *et al.*, 1980). It is also known that in the active center of PPA, successive events like hydrolysis, transglycosylation, and condensation may occur (Robyt & French, 1970a). As a result, various oligomeric molecules can be produced, and different sequences of reaction pathways may be proposed which could happen in the crystal and would give rise to the final product found in our complex structure. The resulting ligand observed probably has the highest affinity for the PPA binding site because its structure is suitable to occupy the whole enzyme binding region with the acarviosine unit at the catalytic center. This agrees with the fact that the strongest inhibition of amylase is associated with components of higher molecular weight than the acarbose molecule (Schmidt *et al.*, 1981).

As shown in the above description, the major features of protein–carbohydrate interactions analyzed by Quiocho (1989) and Vyas (1991) are present in the PPA/acarbose complex. Namely, one can identify three types of hydrogen bonds, stacking interactions, the occurrence of carboxylate side chains and their role in catalysis, and the presence of ordered water

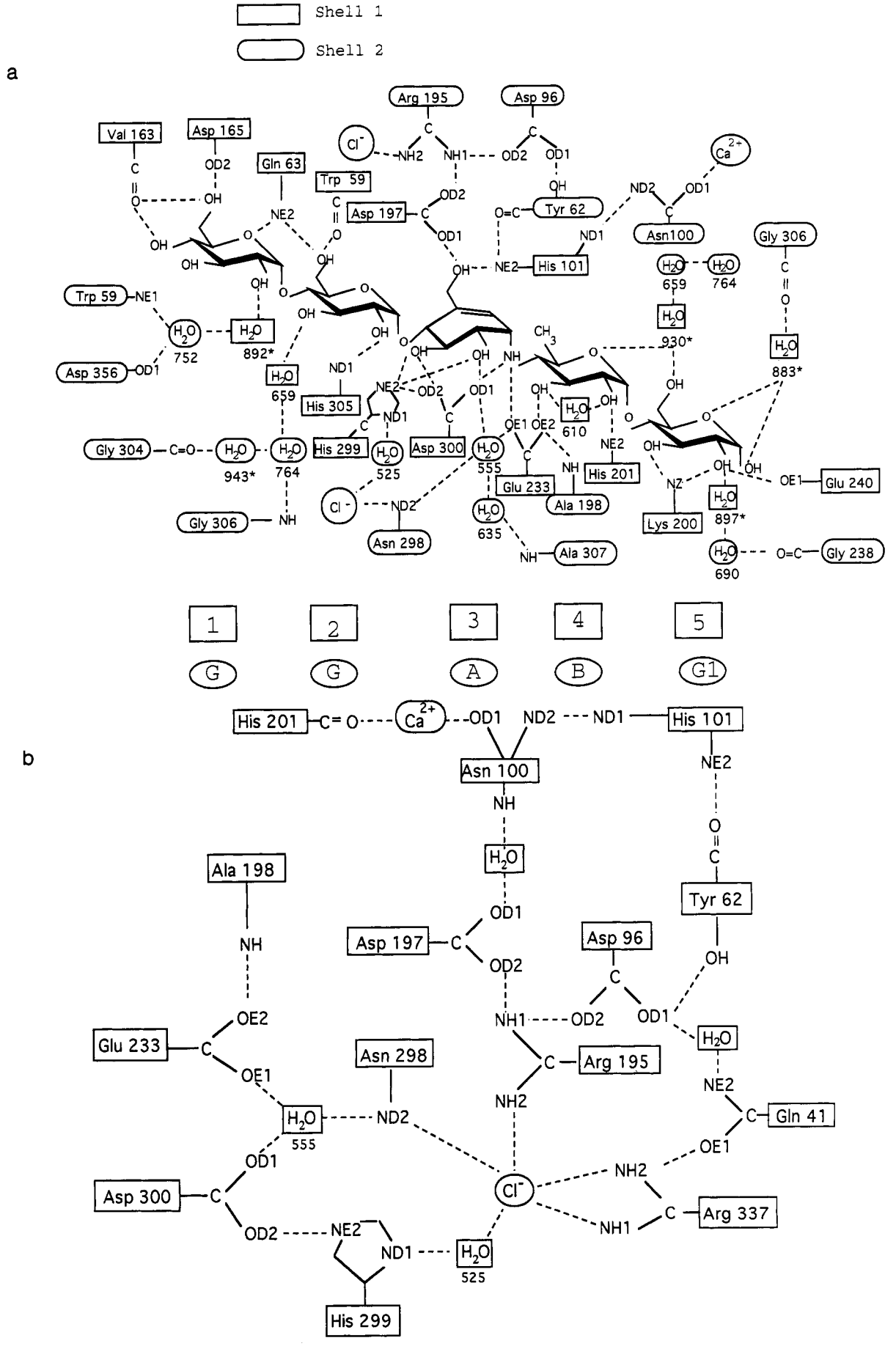

FIGURE 8: (a) Schematic diagram of the hydrogen-bonding network in the active site of the PPA/acarbose complex. The chloride ion is shown in interaction with some of its ligands (Arg195, Asn298, and H_2O). The calcium ion is also shown. The subsites are numbered 1–5 and labeled as explained above (Figure 1a–c). The asterisks indicate water molecules only present in the complexed state. (b) Schematic representation of the network of interactions involving the calcium and chloride ions within the catalytic center.

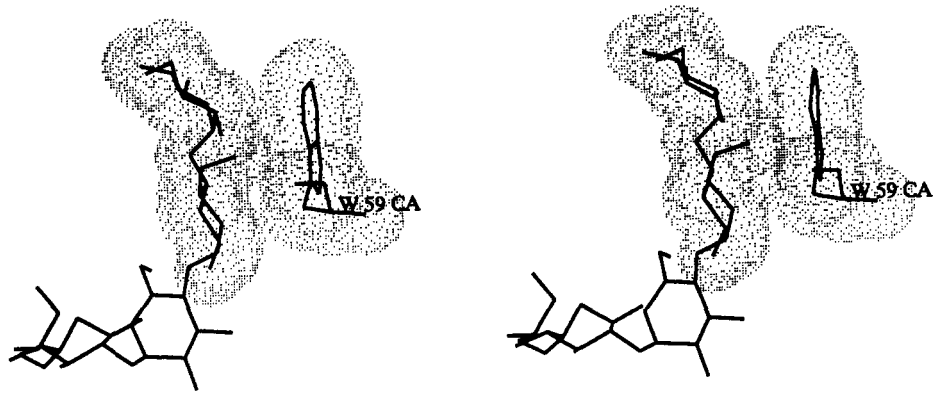

FIGURE 9: Stacking feature between the plane of the tryptophan ring of residue 59 and the hydrophobic region of the maltose unit bound at sites 1 and 2 in the PPA/acarbose complex. Dotted surface represents the van der Waals radii of the atoms.

molecules mediating hydrogen bonds between carbohydrate and protein. Ligand-induced conformational changes bringing into position functional groups for binding and/or catalysis are also observed.

The kink configuration of the ligand observed in the present study seems dictated by the protein environment and enhanced by the ligand length. Significant perturbations of the preferred geometry with torsional flexibilities presumably allowing saccharides to better fit into the binding pocket have also been observed in other carbohydrate–protein interactions (Johnson *et al.*, 1988; Vyas, 1991).

In the X-ray crystallographic studies of the acarbose–phosphorylase *a* complex (Goldsmith *et al.*, 1987), the bound acarbose molecule is stabilized by a series of O2–O3 hydrogen bonds between the O-2 hydroxyl of one sugar and the O-3 hydroxyl of an adjacent sugar. Particularly, concerning the partially ordered cyclitol moiety, the O2–O3 hydrogen bond between the cyclitol and its neighboring sugar is proposed to be responsible for the observed order. In the PPA/acarbose complex, only the torsion angles at the α-(1,4)-*O*-glycosidic bonds connecting sugar residues in subsites 1 and 2 and those in subsites 4 and 5 allow formation of O2–O3 hydrogen bonds, in agreement with the favored geometry of maltose and amylose polymers (Johnson *et al.*, 1988; Quiocho, 1989). The conformation observed for the bound acarviosine (rings A and B) prevent the formation of such a hydrogen bond and breaks the preferred helical conformation.

In the TAKA-amylase three-dimensional structure (Matsuura et al., 1984), the active site has been located in binding studies with maltotriose. Only a disaccharide maltose was observed in a difference density map. It has the OH3 of one glucose unit hydrogen-bonded to O-5 of the next sugar.

Thorough understanding of the interactions of the PPA enzyme with carbohydrates will be completed by analysis of further structure–function studies currently underway.

(b) Protonation State of the Key Active Center Residues. The nitrogen of the amino sugar makes two hydrogen bonds with OD1 of Asp300 and OE1 of Glu233. The arrangement of neighbors around this nitrogen is very close to the tetrahedral coordination; therefore, it is unlikely that both carboxyl groups accept the same hydrogen in two bifurcated hydrogen bonds, but rather there are two protons in this bonding pattern. The acarbose molecule is known to exhibit weakly basic properties, i.e., it is able to accept one more proton from the solvent. Comparison of the two hydrogen bond geometries allows us to conclude that OE1 of Glu233 is more likely to be protonated. Its hydrogen bond is shorter than that from Asp300 by 0.2 Å, and the orientation of the bond within the OCO plane is more appropriate for donating a proton. As mentioned regarding the structure of the native enzyme (Qian *et al.*, 1993), it must be noted that OE1 of Glu233 is close to the chloride ion (the distance is 4.8 Å) and that there are no shielding groups between them. Strong electrostatic interaction between these two negatively charged atoms can shift the p*K* of the carboxyl group of Glu233 to considerably higher values.

His101 is most probably in a neutral state, its ND1 atom accepting a proton from the side-chain nitrogen of Asn100. This unusual hydrogen-bonding probably is due to the close proximity of the Ca ion, which is liganded with N100–OD1 (Qian *et al.*, 1993). The second nitrogen of His101 forms an hydrogen bond with the peptide oxygen of Tyr62. One may note that the p*K* of this histidine residue might be shifted downward because of the close proximity of the Ca ion.

The side chain of Asp197 is most probably deprotonated. It accepts several protons from neighboring groups, including one from O-6 of the cyclitol in subsite 3. Assignment of this proton is unambiguous since in its other hydrogen bond this hydroxyl accepts a proton from NE2 of His101.

The hydrogen-bonding pattern of His201 suggests that this residue is in the protonated state. It is strongly bound to the main-chain oxygen of Val157 with its ND1 and makes another good hydrogen bond (2.7 Å) with the C-2 hydroxyl group of the amino sugar in the fourth subsite. Both of these bonds have an ideal geometry with linear arrangement of ligands in the plane of the imidazole ring. The C-2 hydroxyl group donates its proton to water 610, which in turn donates two protons to the peptide oxygen of Glu233 and the C-3 hydroxyl group of the amino sugar. This chain of bonds cannot be reversed because the latter hydroxyl donates its proton to OE2 of Glu233 and because the orientation of ligands around water 610 is incompatible with the alternative assignment.

The protonation state of another histidine in the proximity of the catalytic center, His299, is ambiguous owing to the complex hydrogen-bonding pattern involving ND1 and NE2 (Figure 8).

(c) Possible Function of Protein Groups in Catalysis. A number of researchers proposed catalytic mechanisms for α-amylases: Koshland (1954), Mayer and Larner (1958), Thoma (1968), Wakim (1969), Fisher and Stein (1960), Tao *et al.* (1989), and Ishikawa (1990). The first mechanism suggested (Koshland, 1954) consisted of a nucleophilic displacement. A double-step mechanism was proposed, where the intermediate state involved in the process was a covalently bonded structure. This mechanism was completed (Fisher & Stein, 1960) by inclusion of a carboxylate anion as the nucleophilic catalytic group. Tao *et al.* (1989) reported a nuclear magnetic resonance study supporting the double-displacement mechanism with the formation of a β-carboxyl acetal ester covalent enzyme–glycosyl intermediate.

As an alternative, Mayer and Larner (1958) proposed a mechanism with an acid-type hydrolysis, giving a carbonium ion intermediate which is stabilized by the enzyme, and stereospecific hydration of the intermediate to form products. Later, a general acid–base mechanism was proposed by Phillips and co-workers (Phillips, 1966; Blake *et al.*, 1967a,b) for enzyme hydrolysis of *O*-glycosidic bonds by lysozyme. A highly refined X-ray structure of an inhibitor complex of hen egg white lysozyme (Strynadka & James, 1991) provided evidence for the transfer of a proton from a glutamic carboxyl (Glu35) to the glycosidic oxygen atom and for an oxocarbonium ion transition state. At present, this mechanism is considered as the most probable for other glycoside hydrolases including amylases.

Considering the unusually high pH-optimum of pig pancreatic α-amylase, which occurs in a neutral pH range, Thoma (1968) and Wakim *et al.* (1969) proposed that a histidine residue may act as a general acid, since a high pK value allows its imidazole ring to be protonated at physiological pH. Recently this hypothesis was elaborated by Ishikawa *et al.* (1990). These authors suggested that at least three ionizable residues are involved in the catalytic function of PPA, with a histidine acting as a proton donor.

Our results provide details of the relative disposition of atoms in an α-amylase–inhibitor complex that can help in considering various reaction mechanisms. The acarbose complex does not provide evidences of a covalent enzyme–glycosyl intermediate. Fisher and Stein (1960) employed a carboxylate anion as the nucleophile in a double-displacement catalytic scheme. Considering our crystallographic results, one may note that, indeed, the positions of both Asp197 and Glu233 in principle allow them to be the nucleophilic partner of the reaction and to produce the β-linked glycosyl–enzyme intermediate. However, in the acarbose complex structure, OD2 of Asp197 is located at 3.3 Å and OE2 of Glu233 at 3.5 Å from the anomeric C-1 atom of the scissible bond, which are approximately 1.8 Å longer than the expected covalent bonds. Moreover, the *B*-factors of the surrounding protein atoms in the free as well as in the complexed structures are very low, indicating low mobility of this region.

Acarbose is thought to be a transition-state analogue in glycosidase catalysis because of the half-chair conformation of the cyclitol ring resembling the conformation of the oxocarbonium ion (Goldsmith *et al.*, 1987; Schmidt *et al.*, 1977). As a matter of fact, the structural arrangement observed in the acarbose complex indicates that the necessary requirements for hydrolysis *via* the general acid hydrolysis mechanism can be satisfied in the PPA structure. The carboxyl groups of Glu233 and Asp300 are perfectly oriented for the transfer of a proton to the glycosidic oxygen atom. Our results suggest that Glu233 is the most appropriate candidate for the role of the general acid in the first stage of the catalytic process. Its pK value must be additionally increased with respect to that of the neighboring aspartic residues because it is very close to the negative chloride ion.

In recent years, functional roles of histidine residues in HPA (very homologous to PPA) have been examined by protein engineering, where the histidine residues His101, His201, and His299 were converted to respective asparagine residues (Ishikawa *et al.*, 1993). The homologous histidine residues in CGTase from alkalophilic *Bacillus* sp. 1011 (His140, His233, and His327) were also replaced by site-directed mutagenesis to prove their roles in catalysis (Nakamura *et al.*, 1993). The first work led to the conclusion that His101 and His299 play an important role in catalysis, His101 being most directly involved in catalysis. For CGTase it was shown that His327 contributed directly or indirectly to the catalysis over an alkaline pH range.

It is clear from our results that none of the above three histidine residues found to be conserved in all α-amylase and CGTase sequences (MacGregor & Svensson, 1989) can act directly as a proton donor, as proposed by some authors (Thoma, 1968; Wakim *et al.*, 1969; Ishikawa *et al.*, 1990). The inhibitor complex structure shows, however, that after inhibitor binding, His299 becomes closely attached to Asp300, suggesting that it can be indirectly involved in the function of the catalytic carboxyl group. Substitution of H299N by site-directed mutagenesis in HPA dramatically decreases its activity, although it does not inactivate the enzyme (Ishikawa *et al.*, 1993). A stronger effect was observed for *Bacillus* sp. 1011 CGTase when the analogous H327N substitution was made (Nakamura *et al.*, 1993). Ishikawa *et al.* (1993) also reported that the HPA mutant H101N has a much lower activity compared to that of H299N mutant and hypothesized that His101 plays a major role in catalysis. According to our data, however, His101 hardly can be involved in some proton-transfer reactions in the catalytic center. Its protonation state probably is fixed, because its ND1 atom has an acceptor function in the hydrogen-bonding with a Ca ion ligand, namely Asn100. The only possible explanation for the results by Ishikawa *et al.* (1990, 1993) that one can propose from our structural data is that the hydrogen bond made by His101 with the cyclitol ring in subsite 3 may be particularly important for the stabilization of the intermediate state of the glucose residue in the catalytic subsite.

The binding of a chloride ion to mammalian α-amylases causes an increase in their activities and a shift of their optimum pH to neutrality (Wakim *et al.*, 1969; Levitzki & Steer, 1974). The structural arrangement of the active site in the acarbose complex structure, in which a number of protein residues are involved in a hydrogen bond network with the chloride ion, suggests that this ion stabilizes the region and may play a regulator role in the catalytic mechanism. Based upon our data, the observed shift of the pH-optimum may be attributed to the electrostatic repulsion between the chloride and the negative charge on the side chain of Glu233. This interaction should stabilize the protonated state of this residue, thus increasing its pK value. This explanation agrees with the suggested role of Glu233 as a proton donor in the catalytic mechanism.

A new structural feature found in the present study is the motion of the loop involving His305 (Figure 5). This histidine residue is not conserved in TAKA-amylase as well as in most of the other amylase and CGTase sequences (MacGregor & Svensson, 1989), but it is conserved in mammalian α-amylase sequences (Pasero *et al.*, 1986). In the TAKA-amylase structure, the homologous loop region is very small, and it does not protrude into the active site (Swift *et al.*, 1991). Owing to the loop movement, the opening of the active center cleft becomes rather narrow in the inhibitor complex of PPA, and the bound fragment of the substrate analogue becomes partially protected from solvent. As a result, the substrate in PPA might be more tightly bound in all five subsites of the active site region than in the other α-amylases of fungal, plant, and bacterial origins. One can suggest that this loop movement is involved in specific aspects of the PPA mechanisms, such as the multiple attack process which appears to be relevant only for mammalian α-amylases. It may also have a role in the last stages of hydrolysis, when the newly formed product needs to be released. Since the loop is hydrogen-bonded to product molecules from the solvent side, the products may be pulled out from the active center cleft when the loop returns

to its initial conformation. The experimental and theoretical studies devoted to pancreatic amylases are numerous, and in the present paper we were not able to consider them all in detail. For instance, such features as substrate dependence of pH profiles (Ishikawa *et al.*, 1990) and the multiple attack mechanism of PPA (Robyt & French, 1970b; Mazur & Nakatani, 1993) require separate analysis and probably model-building studies based upon the inhibitor complex structure.

Our results provide the first atomic description of the interaction between a mammalian α-amylase and its inhibitor, and they give an accurate basis for further theoretical developments on the subject.

ACKNOWLEDGMENT

We wish to thank Dr. H. Bischoff (BAYER AG) for supplying acarbose, Prof. G. Marchis-Mouren for supplying us with α-amylase, Dr. A. K. Mazur (Russian Academy of Sciences), and Drs. H. van Tilbeurgh, C. Cambillau, and Y. Bourne (LCCMB) for critical reading of the manuscript. We also thank Prof. N. H. Xuong and his group for assistance in data collection.

REFERENCES

Blake, C. C. F., Mair, G. A., North, A. C. T., Phillips, D. C., & Sarma, V. R. (1967a) *Proc. R. Soc. London Ser. B 167*, 365–377.

Blake, C. C. F., Johnson, L. N., Mair, G. A., North, A. C. T., Phillips, D. C., & Sarma, V. R. (1967b) *Proc. R. Soc. London Ser. B 167*, 378–388.

Bock, K., & Pedersen, H. (1984) *Carbohydr. Res. 132*, 142–149.

Brady, R. L., Brzozowski, A. M., Derewenda, Z. S., Dodson, E. J., & Dodson, G. G. (1991) *Acta Crystallogr. B47*, 527–535.

Braun, P. J., French, D., & Robyt, J. F. (1985a) *Carbohydr. Res. 141*, 265–271.

Braun, P. J., French, D., & Robyt, J. F. (1985b) *Arch. Biochem. Biophys. 242*, 231–239.

Brünger, A. T., Kuriyan, J., & Karplus, M. (1987) *Science 35*, 458–460.

Chan, Y. C., Braun, P. J., French, D., & Robyt, J. F. (1984) *Biochemistry 23*, 5795–5800.

Fisher, E. H., & Stein, E. A. (1960) in *The Enzymes* (Boyer, P. D., Lardy, H., & Myrbach, K., Eds.) Vol. 4, pp 313–343, Academic Press Inc., New York.

Goldsmith, E. J., Fletterick, R. J., & Withers, S. G. (1987) *J. Biol. Chem. 262*, 1449–1455.

Hamlin, R. (1985) *Methods Enzymol. 114*, 416–452.

Ishikawa, K., Matsui, I., & Honda, K. (1990) *Biochemistry 29*, 7119–7123.

Ishikawa, K., Matsui, I., Kobayashi, S., Nakatani, H., & Honda, K. (1993) *Biochemistry 32*, 6259–6265.

Johnson, L. N., Cheetham, J., McLaughlin, J. P., Acharya, K. R., Barford, D., & Phillips, D. C. (1988) in *Current topics in microbiology and immunology*, Vol. 139, pp 82–134, Springer-Verlag, Berlin.

Kadziola, A. (1993) Ph.D. Thesis, CNRS-Marseille/University of Copenhagen.

Klein, C., Hollender, J., Bender, H., & Schulz, G. E. (1992) *Biochemistry 31*, 8740–8746.

Kluh, I. (1981) *FEBS Lett. 136*, 231–234.

Koshland, D. E., Jr. (1954) in *Symposium on the mechanism of enzyme action* (McElroy, W. D., & Glass, B., Eds.) pp 608–641, The Johns Hopkins University Press, Baltimore, MD.

Levitzki, A., & Steer, M. L. (1974) *Eur. J. Biochem. 41*, 171–180.

MacGregor, E. A., & Svensson, B. (1989) *Biochem. J. 259*, 145–152.

Marchis-Mouren, G., & Desseaux, V. (1989) *Biochem. Life Sci. Adv. 8*, 91–96.

Marchis-Mouren, G., & Pasero, L. (1967) *Biochim. Biophys. Acta 140*, 366–368.

Matsuura, Y., Kusunoki, M., Harada, W., & Kakudo, M. (1984) *J. Biochem. 95*, 697–702.

Mayer, F. C., & Larner, J. (1958) *Biochim. Biophys. Acta 29*, 465.

Mazur, A. K., & Nakatani, H. (1993) *Arch. Biochem. Biophys. 306*, 29–38.

Müller, L., Junge, B., & Frommer, W. (1980) in *Enzyme Inhibitors* (Brodbeck, U., Ed.) pp 109–122, Verlag Chemie, Weinheim.

Nakamura, A., Haga, K., & Yamane, K. (1993) *Biochemistry 32*, 6624–6631.

Pasero, L., Abadie, B., Chicheportiche, Y., Mazzei, Y., Moinier, D., Bizzozero, J. P., Fougereau, M., & Marchis-Mouren, G. (1981) *Biochimie 63*, 71–79.

Pasero, L., Mazzei-Pierron, Y., Abadie, B., Chicheportiche, Y., & Marchis-Mouren, G. (1986) *Biochim. Biophys. Acta 869*, 147–157.

Payan, F., Haser, R., Pierrot, M., Frey, M., Astier, J. P., Abadie, B., Duée, E., & Buisson, G. (1980) *Acta Crystallogr. B36*, 416–421.

Phillips, D. C. (1966) *Sci. Am. 215*, 78–90.

Prodanov, E., Seigner, C., & Marchis-Mouren, G. (1984) *Biochem. Biophys. Res. Commun. 122*, 75–81.

Qian, M., Haser, H., & Payan, F. (1993) *J. Mol. Biol. 231*, 785–799.

Quiocho, F. A. (1989) *Pure Appl. Chem. 61*, 1293–1306.

Ramachandran, G. N., & Sasisekharan, V. (1968) *Adv. Protein Chem. 23*, 283–437.

Robyt, J. F., & French, D. (1970a) *J. Biol. Chem. 45*, 3917–3927.

Robyt, J. F., & French, D. (1970b) *Arch. Biochem. Biophys. 138*, 622–670.

Roussel, A., & Cambillau, C. (1989) in *Silicon Graphics geometry partner directory (Fall 1989)*, pp 77–78, Silicon Graphics, Mountain View, CA.

Schmidt, D. D., Frommer, B., Junge, L., Müller, W., Wingender, W., & Truscheit, E. (1977) *Naturwissenschaften 64*, 535–536.

Schmidt, D. D., Frommer, B., Junge, L., Müller, W., Wingender, W., & Truscheit, E. (1981) in *First international symposium on Acarbose* (Creutzfeldt, E. W., Ed.) pp 5–15, Excerpta Medica, Amsterdam.

Steer, M., & Levitzki, A. (1973) *FEBS Lett. 31*, 89–92.

Steigemann, W. (1974) Ph.D. Thesis, Technische Universität, München.

Strynadka, N. C. J., & James, M. N. G. (1991) *J. Mol. Biol. 220*, 401–424.

Swift, H. J., Brady, L., Derewenda, Z. S., Dodson, E. J., Dodson, G. G., Turkenburg, J. P., & Wilkinson, A. J. (1991) *Acta Crystallogr. B47*, 535–544.

Tao, B. Y., Reilly, P. J., & Robyt, J. F. (1989) *Biochim. Biophys. Acta 995*, 214–220.

Thoma, J. A. (1968) *J. Theor. Biol. 19*, 297–310.

Thoma, J. A., Spradlin, J. E., & Dygert, S. (1971) in *Enzymes*, 3rd ed., pp 89–115, Academic Press, New York.

Vallee, B. L., Stein, E. A., Summerwell, W. N., & Fisher, E. H. (1959) *J. Biol. Chem. 234*, 2901–2929.

Vyas, N. K. (1991) *Curr. opin. Struct. Biol. 1*, 732–740.

Wakim, J., Robinson, M., & Thoma, J. A. (1969) *Carbohydr. Res. 10*, 487–503.

Wilcox, E. R., & Whitaker, R. J. (1984) *Biochemistry 23*, 1783–1791.